Chapter 5

Haze Removal: Non-Local Haze-line Averaging Based Gradient Guided Image Filter

5.1 Background

The edge-preserving smoothing algorithms are broadly used in many applications of image processing and computer vision such as image dehazing, image enhancement, texture removal and tone mapping of high dynamic range (HDR) images. Generally, the edge-preserving smoothing filters remove haze effect by decomposing haze image into a piecewise base layer and detail layer. The base layer is formed by homogeneous regions with large scale variations in intensity domain while detail layer can be noise or texture. The guided image filter (GIF) and weighted guided image filter (WGIF) are local linear model-based good edge-preserving filters. However, due to fixed regularization parameter, they suffer from halo artifacts (morphological artifacts)

in the sharp regions. In this Chapter, a new robust multi-scale weighting based edge-smoothing filter (RMWEF) is presented for single image dehazing. In this method, a non-local haze line averaging (NL-HLA) algorithm is used to remove the morphological effect strongly and preserve edge details accurately.

The rest of the Chapter is structured as follows. The proposed haze removal algorithm is specified in Section 5.2. Experimental results and analysis are discussed in Section 5.3. Limitations of the proposed method are discussed in Section 5.4 and Section 5.5 concludes the Chapter.

5.1.1 Major Contributions of the Work

The main contributions of this work are as follows:

- In this Chapter, a non-local haze line averaging (NL-HLA) algorithm is used to remove the morphological artifacts. The morphological artifacts are visible, if initial transmission map $\tilde{t}(x, y)$ is used directly to remove haze in the input image.
- Next, a new robust multi-scale weighting based edge-smoothing filter (RMWEF) is proposed for single image dehazing. RMWEF refine the initial transmission map by decomposing it into the base layer (BL) and detail layer (DL), respectively. The proposed filter refines the transmission map more efficiently than the existing GIF [49], WGIF [50], GGIF [51] and EGIF [52] methods.
- The base- and the detail- layer are calculated for four different values of the regularization parameter ε (0.001^2, 0.01^2, 0.1^2, 5^2) and fixed window size $\zeta_1 = 60$.

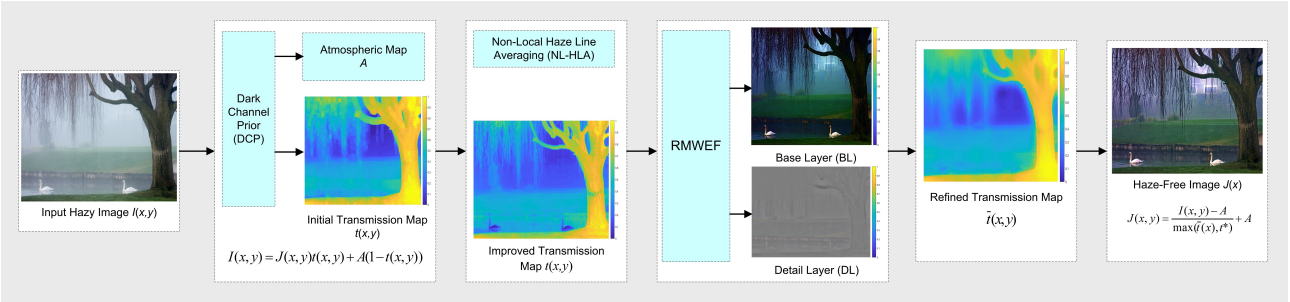

FIGURE 5.1: The flow diagram of the proposed method.

5.2 The Proposed Algorithm

The basic flow-diagram of the proposed algorithm is shown in Figure 5.1. There are, below listed, three steps in the proposed algorithm.

- In the first step, we estimate the atmospheric map and initial transmission map using dark channel prior (DCP) [15] method.
- Next, a non-local haze line averaging (NL-HLA) algorithm is applied on initial transmission map to remove morphological artifacts.
- In the third step, a new robust multi-scale weighting-based edge-smoothing filter (RMWEF) is used to refine the initial transmission map more accurately.
- Finally, haze-free image is retrieved from the scene radiance.

5.2.1 Transmission Map Estimation by Dark Channel Prior (DCP)

The dark channel prior (DCP) [15] method is simple and effective method for estimation of the atmospheric map and transmission map. In DCP [15], dark pixels concept is used to evaluate atmospheric map and transmission map accurately than

the other existing methods. Among these dark pixels, the top 0.1% of brightest pixels are selected for the estimation of atmospheric map as DCP [15]. In the proposed method, dark channel prior (DCP) [15] method is used to estimate the atmospheric map A and initial transmission map $\tilde{t}(x)$. We have already discussed the estimation of the atmospheric map A and initial transmission map $\tilde{t}(x)$ (refer to (3.24)) using DCP in Chapter 3.

$$I^c(x,y) = J^c(x,y)t(x,y) + A^c(1 - t(x,y)), \tag{5.1}$$

where (x,y) is a pixel position and $c \in (R,G,B)$ for color channel. $I^c(x,y)$ is input hazy image, $J^c(x,y)$ is output dehaze image, $t(x,y)$ is the transmission map which describes the amount of light reaching the camera and A is atmospheric map which is constant for the whole image, respectively. The terms $I(x,y)t(x,y)$ and $A^c(1-t(x,y))$ are called direct attenuation and airlight, respectively. The atmospheric- and transmission- maps are estimated using the dark channel prior (DCP) [15] method. The dark channel of an haze-free image ($J(x,y)$) is defined as:

$$J^{dark}(x,y) = \min_{(x',y')\in\omega_{\zeta_1}(x,y)} \Big(\min_c J^c(x',y') \Big), \tag{5.2}$$

where $\omega_{\zeta_1}(x,y)$ is a local square window centred at pixel (x,y) of radius ζ_1. In DCP [15], the transmission map $t(x,y)$ is constant in neighborhood of (x,y) pixels and it is represented by $\tilde{t}(x,y)$. It can be expressed as:

$$\tilde{t}(x,y) = 1 - \min_{(x',y')\in\omega_{\zeta_1}(x,y)} \Big(\min_c \frac{I^c(x,y)}{A^c} \Big). \tag{5.3}$$

5.2.2 Non-Local Haze Line Averaging (NL-HLA)

The morphological artifacts are visible, if initial transmission map $\tilde{t}(x, y)$ is used directly to remove haze from hazy image. Generally, the morphological artifacts are observed due to the usage of DCP and local edge-preserving filters. The concept of the non-local haze line averaging (NL-HLA) [95] is adopted to address this problem. It removes the morphological artifatcs strongly and preserves fine structures precisely. The NL-HLA method first uses the initial transmission map to estimate the distance of each pixel from the origin in the haze free image. Then, it averages the distance of each pixels over a new set of pixels in the same haze line and obtains an improved estimation on the distance of each pixel to the origin in the haze free image. This improved estimation is applied to compute the transmission map.

The morphological artifacts can be derived by (5.1) and (5.3) as:

$$\frac{\tilde{t}(x, y)}{\|\hat{I}(x, y)\|} = \frac{1}{\|J(x, y) - A\|} + E_{rr}(x, y), \tag{5.4}$$

where $E_{rr}(x, y)$ represents the morphological artifacts. In NL-HLA [95], the new set of pixels (x', y') in hazy image I can be expressed as:

$$\frac{1}{\|J(x, y) - A\|} = \frac{1}{\mu_{sum}} \sum_{x', y'} \mu(x', y') \frac{\tilde{t}(x', y')}{\|\hat{I}(x', y')\|}. \tag{5.5}$$

The weighted average in above (5.5) is known as non-local haze line averaging (NL-HLA) [95] where $\mu(x', y')$ represents a weight and μ_{sum} is expressed as:

$$\mu_{sum} = \sum_{x', y'} \mu(x', y'). \tag{5.6}$$

In [95], NL-HLA based transmission map is finally expressed as:

$$t(x,y) = \frac{\sum_{(x',y')\in H_s(x'',y'')} \tilde{t}_(x',y')}{\sum_{(x',y')\in H_s(x'',y'')} \|\hat{I}(x',y')\|} \|\hat{I}(x,y)\|, \tag{5.7}$$

where $H_s(x'', y'')$ is the set of all $I(x, y)$ used to form a haze line [95].

5.2.3 Robust Multi-Scale Weighting-Based Edge-Smoothing Filter (RMWEF)

In this section, a robust multi-scale weighting-based edge-smoothing filter (RMWEF) is proposed to remove morphological artifacts and over-smoothing strongly in both smooth and sharp regions. The GIF [49], WGIF [50], GGIF [51] and EGIF [52] are also fast and effective edge-preserving smoothing filters. They remove halo artifacts and preserve edge information in both flat as well as sharp regions. However, morphological artifacts and over smooth in images increases with increasing of the regularization parameter value. As compared to the existing filters, GGIF [51] is less sensitive to the regularization parameter. Additionally, it removes halo artifacts and preserve edge information in both regions precisely than the existing filters [49], [50], [52]. Therefore, we propose a robust multi-scale weighting-based edge-smoothing filter (RMWEF) to reduce the morphological artifacts.

5.2.4 A New Edge-Aware Weighting

In this section, the proposed multi-scale weighting is defined by normalizing the variances of local window pixels with the average of local variances for all pixels in

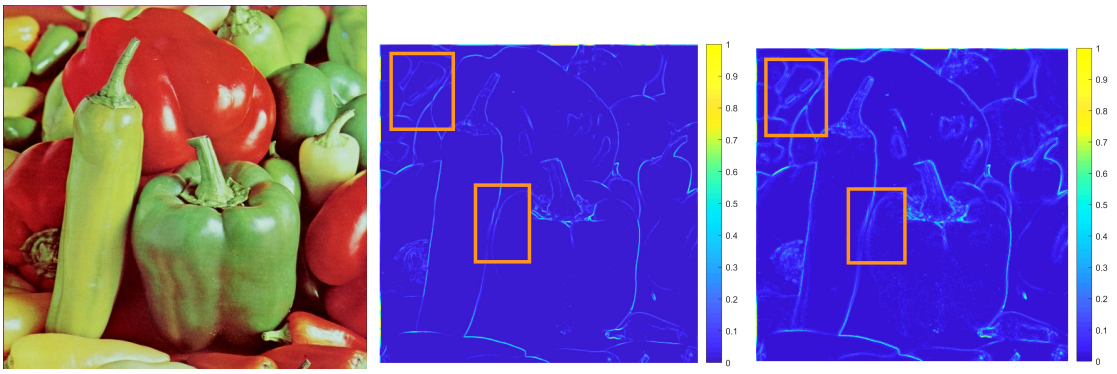

(a) Input [15] (b) $\Gamma_I(x', y')$ [50] (c) $\hat{\Gamma}_I(x', y')$ [51]

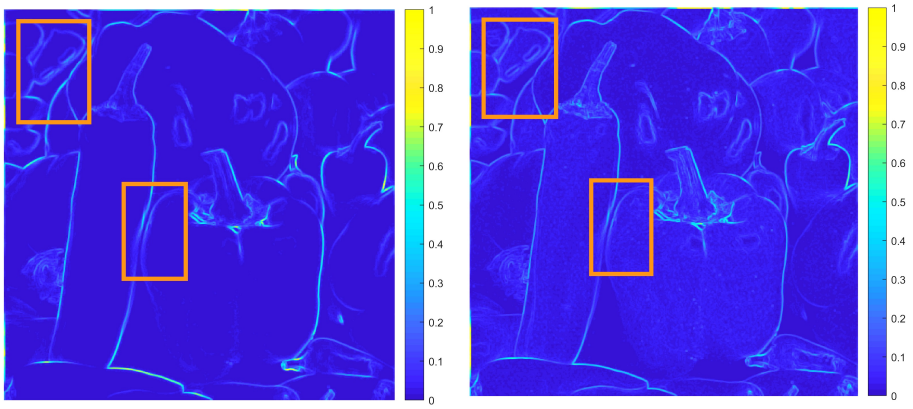

(d) $\overline{\Gamma}_I(x', y')$ [52] (e) The proposed $\overline{\Phi}_I(x', y')$

FIGURE 5.2: Comparison of edge-aware weighting of different haze removal methods. $\zeta_1 = 60$ and $\varepsilon = 0.1^2$ is set for all figures.

an image. It can be expressed as:

$$\overline{\Phi}_I(x', y') = \frac{\sigma_{I,1}(x', y')\sigma_{I,\,\zeta_1}(x', y')}{\overline{\sigma}^2}, \tag{5.8}$$

where $\overline{\sigma}^2 = \frac{1}{N}\sum_1^N {\sigma^2}_{I,\,\zeta_1}(x', y')$ is an average variance for all pixels and $\sigma_{I,1}(x', y')\sigma_{I,\,\zeta_1}(x', y')$ is local variance in window $\omega_{\zeta_1}(x', y')$. The window radius $\zeta_1 = 60$ is used to reduce the morphological artifacts strongly and preserve the fine structures precisely. Similar to GIF [49] and WGIF [50], the computation complexity of $\overline{\Phi}_I(x', y')$ is $O(N)$ for an image with N pixels. Figure 5.2 illustrate the comparison of edge-aware weights $\Gamma_I(x', y')$, $\hat{\Gamma}_I(x', y')$, $\overline{\Gamma}_I(x', y')$ and $\overline{\Phi}_I(x', y')$. In this figure, we have set $\zeta_1 = 60$ and $\varepsilon = 0.1^2$ to compute the edge-aware weighting of existing edge-preserving filters

and the proposed method. It is evident from these figures that the proposed edge-aware weighting detect edges more precisely and clearly than the existing WGIF [50], GGIF [51] and EGIF [52] methods.

5.2.5 The Proposed RMWEF

The cost function in the proposed RMWEF is minimized by linear ridge regression model [63, 64]. The values of linear coefficients $a_{x',y'}$ and $b_{x',y'}$ are evaluated by minimizing the cost function $E(a_{x',y'}, b_{x',y'})$ in the window $\omega_{\zeta_1}(x', y')$ as:

$$E(a_{x',y'}, b_{x',y'}) = \sum_{(x,y)\in\omega_{\zeta_1}(x',y')} [(a_{x',y'}I_{\mathrm{x,y}} + b_{x',y'} - p_{x,y})^2 + \frac{\varepsilon}{\overline{\Phi}_I(x',y')}(a_{x',y'} - \gamma_{x',y'})^2]. \tag{5.9}$$

The optimized value of linear coefficients $a_{x',y'}$ and $b_{x',y'}$ are calculated by the following expression:

$$a_{x',y'} = \frac{\mu_{I\odot p,\ \zeta_1}(x',y') - \mu_{I,\ \zeta_1}(x',y')\ \mu_{p,\ \zeta_1}(x',y') + \frac{\varepsilon}{\overline{\Phi}_I(x',y')}\gamma_{x',y'}}{{\sigma^2}_{I,\ \zeta_1}(x',y') + \frac{\varepsilon}{\overline{\Phi}_I(x',y')}}, \tag{5.10}$$

and

$$b_{x',y'} = \mu_{p,\ \zeta_1}(x',y') - a_{x',y'}\mu_{I,\ \zeta_1}(x',y'). \tag{5.11}$$

For better analysis, I and p can be assumed identical and it can be expressed after simplification as:

$$\mu_{I\odot p,\ \zeta_1}(x',y') - \mu_{I,\ \zeta_1}(x',y')\ \mu_{p,\ \zeta_1}(x',y') = {\sigma^2}_{I,\ \zeta_1}(x',y') \tag{5.12}$$

and

$$\mu_{p,\ \zeta_1}(x',y') = \mu_{I,\ \zeta_1}(x',y'). \tag{5.13}$$

After substituting (5.12) and (5.13) into (5.10) and (5.11), respectively. We obtain

$$a_{x',y'} = \frac{\sigma^2{}_{I,\,\zeta_1}(x',y') + \frac{\varepsilon}{\overline{\Phi}_I(x',y')}\gamma_{x',y'}}{\sigma^2{}_{I,\,\zeta_1}(x',y') + \frac{\varepsilon}{\overline{\Phi}_I(x',y')}}, \tag{5.14}$$

and

$$b_{x',y'} = (1 - a_{x',y'})\mu_{I,\,\zeta_1}(x',y'). \tag{5.15}$$

Finally, the filter output $q_{x,y}$ is obtained after substituting $a_{x',y'}$ and $b_{x',y'}$ values from (5.14) and (5.15) into the (5.16). It can be expressed as:

$$q_{x,y} = a_{x',y'}I_{x,y} + b_{x',y'}, \forall (x,y) \in \omega_{\zeta_1}(x',y'). \tag{5.16}$$

Finally, it can be expressed as:

$$q_{x,y} = \frac{1}{|\omega_{\zeta_1}(x,y)|} \sum_{(x',y')\in\omega_{\zeta_1}(x,y)} (a_{x',y'}I_{x,y} + b_{x',y'}), \tag{5.17}$$

$$q_{x,y} = (\overline{a}_{x,y}I_{x,y} + \overline{b}_{x,y}), \tag{5.18}$$

where $\overline{a}_{x,y}$ and $\overline{b}_{x,y}$ terms in the (5.18) represent average or mean of $a_{x',y'}$ and $b_{x',y'}$, respectively and it can be expressed as:

$$\overline{a}_{x,y} = \frac{1}{|\omega_{\zeta_1}(x,y)|} \sum_{(x',y')\in\omega_{\zeta_1}(x,y)} a_{x',y'}, \tag{5.19}$$

$$\overline{b}_{x,y} = \frac{1}{|\omega_{\zeta_1}(x,y)|} \sum_{(x',y')\in\omega_{\zeta_1}(x,y)} b_{x',y'}. \tag{5.20}$$

Usually following two cases are of more interest:

- According to GGIF [51], to preserve edge information in the sharp region, $a_{x',y'}$ should reduce to 1. Therefore, evaluating (5.14) with $\gamma_{x',y'} = 1$:

$$a_{x',y'} = \frac{\sigma^2{}_{I,\,\zeta_1}(x',y') + \frac{\varepsilon}{\overline{\Phi}_I(x',y')}}{\sigma^2{}_{I,\,\zeta_1}(x',y') + \frac{\varepsilon}{\overline{\Phi}_I(x',y')}} = 1. \tag{5.21}$$

- For smooth region, $a_{x',y'}$ should be 0 (zero). Therefore, evaluating (5.14) with $\gamma_{x',y'} = 0$: After substituting this condition in (5.14), $a_{x',y'}$ can be expressed as:

$$a_{x',y'} = \frac{\sigma^2{}_{I,\,\zeta_1}(x',y')}{\sigma^2{}_{I,\,\zeta_1}(x',y') + \frac{\varepsilon}{\overline{\Phi}_I(x',y')}}. \tag{5.22}$$

  Thus, we obtain $a_{x',y'} = 1$ for $\gamma_{x',y'} = 1$ (sharp region) and it is close to 0 for $\gamma_{x',y'} = 0$ (smooth region), as expected.

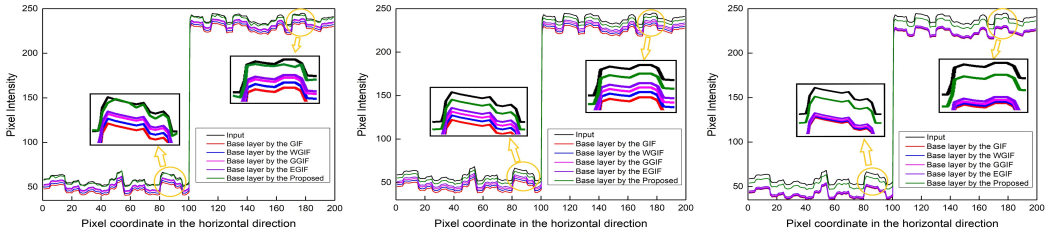

(a) (b) (c)

FIGURE 5.3: 1-D illustration between pixel intensity and pixel coordinates in the horizontal directions for tulip image shown in Figure 5.5. For all figures, $\zeta_1 = 60$ set and ε is changed. (a) $\varepsilon = 0.01^2$, (b) $\varepsilon = 0.1^2$, (c) $\varepsilon = 1^2$.

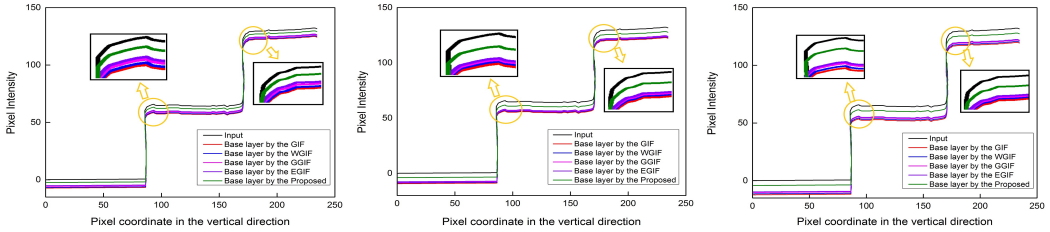

(a) (b) (c)

FIGURE 5.4: 1-D illustration between pixel intensity and pixel coordinates in the vertical directions for tulip image shown in Figure 5.5. For all figures, $\zeta_1 = 60$ set and ε is changed. (a) $\varepsilon = 0.01^2$, (b) $\varepsilon = 0.1^2$, (c) $\varepsilon = 1^2$.

Next, the 1-D illustration between pixel intensity and pixel coordinates in the horizontal as well as in the vertical directions for tulip image are calculated. Figure 5.3 (a)-(c) depicts 1-D illustration between pixel intensity and pixel coordinates in the horizontal direction for GIF [49], WGIF [50], GGIF [51], EGIF [52] and the proposed method at $\zeta_1 = 60$ for three different ε values 0.01^2, 0.1^2, and 1^2, respectively. Similarly, Figure 5.4 represents the 1-D illustration between pixel intensity and pixel coordinates in the vertical direction. It is clear from zoomed-in patches illustrated in Figure 5.3 (a)-(c) and Figure 5.4 (a)-(c) that the output pixel values of the proposed method are more closer to the input pixel values even with large ε values, whereas those are far apart in case of the other existing methods. Therefore, it can be conjectured that the proposed method removes halo artifacts strongly and preserves edge information precisely in both flat as well as sharp regions.

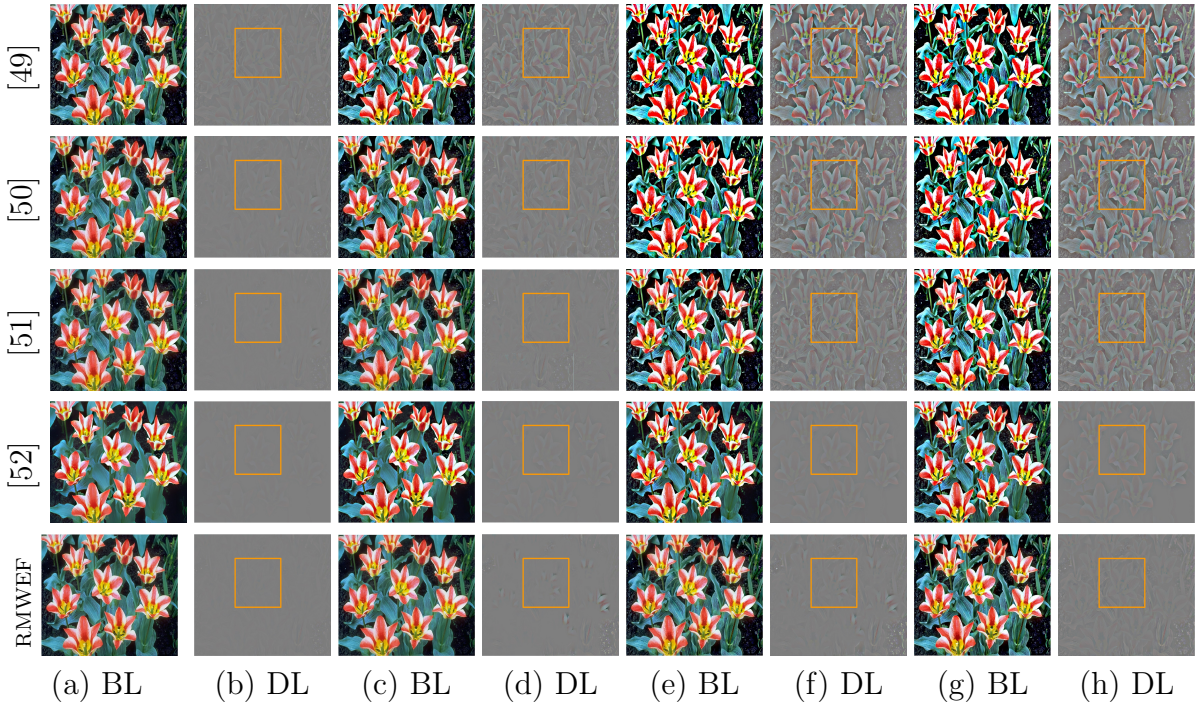

FIGURE 5.5: Visual comparison of the base layer (BL) and detail layer (DL) on tulip image. For all figures, $\zeta_1 = 60$ set and ε is changed. (a) and (b) $\varepsilon = 0.001^2$, (c) and (d) $\varepsilon = 0.01^2$, (e) and (f) $\varepsilon = 0.1^2$, (g) and (h) $\varepsilon = 5^2$.

5.2.6 Transmission map Refinement by RMWEF

In this section, the NL-HLA based initial transmission map is refined by the proposed RMWEF algorithm and can be expressed as:

$$t(x,y) = a_{x',y'} I(x,y) + b_{x',y'}, \forall (x,y) \in \omega_{\zeta_1}(x',y'). \tag{5.23}$$

The optimal values of linear coefficients $a_{x',y'}$ and $b_{x',y'}$ are derived by minimizing the cost function as used in [49] can be defined as:

$$E(a_{x,y}, b_{x,y}) = \sum_{(x,y)\in\omega_{\zeta_1}(x',y')} [(a_{x',y'} I(x,y) + b_{x',y'} - t(x,y))^2 + \frac{\varepsilon (a_{x',y'} - \gamma_{x',y'})^2}{\overline{\Phi}_{x',y'}}], \tag{5.24}$$

where $\overline{\Phi}_{x',y'}$ is the proposed multi-scale edge-aware weighting, $\gamma_{x',y'}$ is an edge-aware smoothing parameter. After estimation of optimal values of $a_{x',y'}$ and $b_{x',y'}$, the refined transmission map can be expressed as:

$$\overline{t}(x,y) = \overline{a}_{x,y} I(x,y) + \overline{b}_{x,y}, \forall (x,y) \in \omega_{\zeta_1}(x',y'), \tag{5.25}$$

where $\overline{a}_{x,y}$ and $\overline{b}_{x,y}$ are the average values of $a_{x',y'}$ and $b_{x',y'}$, respectively in the square window $\omega_{\zeta_1}(x,y)$. Generally, the edge-preserving smoothing techniques can decompose an image into a piecewise smooth base layer which is large scale variation in pixel intensity while the detail layer can be computed after taking difference between input and output image. The base- and the detail- layer for a non-hazy tulip image [50] is calculated the proposed method for four different values of regularization parameter $\varepsilon = 0.001^2$, $\varepsilon = 0.01^2$, $\varepsilon = 0.1^2$, $\varepsilon = 5^2$ and comparison result with GIF [49], WGIF [50], GGIF [51] and EGIF [52] is shown in Figure 5.5.

The halo artifacts and over-smoothing effects in GIF [49], WGIF [50], GGIF [51]

and EGIF [52] increase with increasing of the regularization parameter (ε) and it produces more details (textures) in the detail layer for large ε value. It can be observed from Figure 5.5 that the details (textures) are prominent in the detail layer for large ε values and cause more artifacts. On the contrary, the outcomes of the proposed method has less details in the detail layer even with large ε values than the existing methods. The base layers of GIF [49], WGIF [50], GGIF [51] and EGIF [52] get more enhanced for large ε values and create black halos around the sharp regions, whereas the base layer of the proposed method is free from these artifacts. This entails that the proposed method removes halo artifacts strongly and avoid over smooth in images even for large regularization parameter.

5.2.7 Restoration of the Haze-Free Image

Once the atmospheric map (A) and the refined transmission map $\bar{t}(x)$ are obtained, haze-free image can be recovered by the following expression:

$$J^c(x,y) = \frac{I^c(x,y) - A^c}{max(\bar{t}(x,y), t^*)} + A^c, \tag{5.26}$$

where t^* is a constant and it is set to 0.1.

5.3 Experimental Results Discussion

The proposed RMWEF is implemented and experimented using Matlab R2015a on a PC with Intel (R) Core (TM) i5-4210U, CPU @ 1.70 GHz of a 64-bit operating system with RAM-8GB. The proposed haze removal algorithm is tested on different sets of hazy, non-hazy, and synthetic images to verify its effectiveness. The images

from realistic single image dehazing (RESIDE) dataset [73] is used to show the effectiveness of the proposed method. The complete RESIDE dataset is divided into five subsets namely; Indoor Training Set (ITS), Outdoor Training Set (OTS), Synthetic Objective Testing Set (SOTS), Real-world Task-driven Testing Set (RTTS) and Hybrid Subjective Testing Set (HSTS), respectively. From these datasets, we used 1200 images from ITS, 1500 images from OTS, 1000 images from SOTS, 600 images from RTTS and 20 images from HSTS to test the dehazing performance of the proposed method. Further, Fattal's dataset [16], D-HAZY dataset [65], Middlebury dataset [96], NYU dataset [66], FRIDA dataset [67] are also used for better analysis and the results are compared with the existing dehaze algorithms GIF [49], WGIF [50], EPDSID [61], GGIF [51], EGIF [52], DN [37], RYF-Net [39], PMHLD [41] and IDNPAB [40].

To asses the effectiveness of the proposed algorithm, some of the non-referenced, referenced performance quantitative metrics and the execution time (T/s) are calculated for GIF [49], WGIF [50], EPDSID [61], GGIF [51], EGIF [52], DN [37], RYF-Net [39], PMHLD [41], IDNPAB [40] and the proposed method. The quantitative results obtained for GIF [49], WGIF [50], EPDSID [61], GGIF [51], EGIF [52], DN [37], RYF-Net [39], PMHLD [41], IDNPAB [40] and the proposed method on five subsets of RESIDE dataset namely Indoor Training Set (ITS), Outdoor Training Set (OTS), Synthetic Objective Testing Set (SOTS), Real-world Task-driven Testing Set (RTTS) and Hybrid Subjective Testing Set (HSTS) for three different ε values (0.01^2, 0.1^2, 1^2) and fixed window size $\zeta_1 = 60$ and the results are furnished in Table 5.1. Further, we calculated these performance metrics for various images from Fattal's, D-HAZY, Middlebury, NYU and FRIDA dataset in a similar way and these results are furnished in Table 5.2.

Some image dehazing methods (DN [37], RYF-Net [39], PMHLD [41], IDNPAB [40]) in Table 5.1 and Table 5.2 are independent of regularization parameter and these cases are marked with a $'-'$ in both Tables. The bold values in Table 5.1 and Table 5.2 are indicate the best results. It can be clearly observed from these Tables that the proposed method has the highest e and $\overline{r}$ values and the least $\overline{\alpha}$ value than the rest of the existing methods. Next, it can be clearly observed from Table 5.1 and 5.2 that CNI value for all dehazing methods is higher for natural hazy images. The best CNI values in Table 5.1 and 5.2 are **0.9992, 0.9987**, respectively. Overall, it is evident from Table 5.1 and 5.2 that CNI performance of the proposed method is much closer to 1 as expected than the rest of the methods. Out of five subsets of RESIDE datasets, it is evident from Table 5.1 that the best FADE value **0.05** is obtained with SOTS subset. Similarly, it is evident that the best FADE value **0.07** is obtained with D-HAZY dataset as listed in Table 5.2. It is evident from this analysis that the proposed method performs better in terms of FADE on all types of the images.

Next, higher peak signal to noise ratio (PSNR) and structural similarity index (SSIM) value represent the corresponding image has higher image quality. As shown in Table 5.1 and Table 5.2 that the best PSNR and SSIM values are **38.85, 39.51** and **0.8891, 0.8945**, respectively. This fact can also be validated from the quality of images shown in Figure 5.6 to 5.8. It is clear from these results that the proposed method has higher PSNR and SSIM values than the existing GIF [49], WGIF [50], EPDSID [61], GGIF [51], EGIF [52], DN [37], RYF-Net [39], PMHLD [41], IDNPAB [40] methods. Further, lower value of CIEDE2000 metric indicates better color preservation in the restored image. It is evident from Table 5.1-5.2 that the best CIEDE2000 values are obtained with the proposed method than the rest of the methods, as expected. As shown in Table 5.1-5.2 that the best UIQI values are

0.9772, 0.9771 and these are obtained with the proposed method. Therefore, it can be concluded from this quantitative analysis that the performance of the proposed method is the best.

The execution time T/s of the proposed method is compared with the existing methods for images with different resolutions. The resolutions of four benchmark images in Figure 5.6-5.8 are 185 $\times$ 260, 375 $\times$ 512, and 810 $\times$ 1100, respectively. As shown in Table 5.1-5.2 that the execution time of the existing methods and the proposed method depends on the image resolution and it increases with increase in image resolution. The proposed method is faster than the existing methods for a given resolution of images. Overall, it can be concluded that the proposed method strongly removes halo artifacts and preserves edge information more accurately than the existing GIF [49], WGIF [50], EPDSID [61], GGIF [51], EGIF [52], DN [37], RYF-Net [39], PMHLD [41], IDNPAB [40] methods. Moreover, it is independent of the nature of images.

(a) Input 1 (b) GIF (c) WGIF

(d) EPDSID (e) GGIF (f) EGIF

(g) DehazeNet (h) RYFNet (i) PMHLD

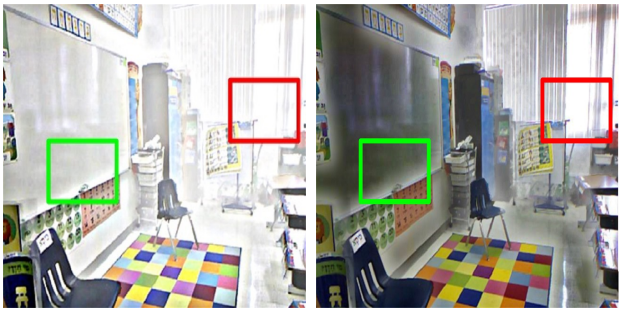

(j) IDNPAB (k) RMWEF

FIGURE 5.6: Visual comparison of different dehaze methods for RESIDE dataset

(a) Input 2 (b) GIF (c) WGIF

(d) EPDSID (e) GGIF (f) EGIF

(g) DehazeNet (h) RYFNet (i) PMHLD

(j) IDNPAB (k) RMWEF

FIGURE 5.7: Visual comparison of different dehaze methods for RESIDE dataset

(a) Input 3 (b) GIF (c) WGIF

(d) EPDSID (e) GGIF (f) EGIF

(g) DehazeNet (h) RYFNet (i) PMHLD

(j) IDNPAB (k) RMWEF

FIGURE 5.8: Visual comparison of different dehaze methods for RESIDE dataset

Table 5.1: Comparison of the average performance metrics and execution time using different dehazing methods for three different ε values $(0.01^2, 0.1^2, 1^2)$ and fixed $\zeta_1 = 60$ for RESIDE Dataset.

RESIDE Dataset	Methods	Non-Reference Metrics															Reference Metrics												Execution Time		
		e			$\bar{r}$			$\bar{\sigma}$			CNI			FADE			PSNR			SSIM			CIEDE2000			UIQI			T/s		
		$\varepsilon=0.01^2$	$\varepsilon=0.1^2$	$\varepsilon=1^2$	$\varepsilon=0.01^2$	$\varepsilon=0.1^2$	$\varepsilon=1^2$	$\varepsilon=0.01^2$	$\varepsilon=0.1^2$	$\varepsilon=1^2$	$\varepsilon=0.01^2$	$\varepsilon=0.1^2$	$\varepsilon=1^2$	$\varepsilon=0.01^2$	$\varepsilon=0.1^2$	$\varepsilon=1^2$	$\varepsilon=0.01^2$	$\varepsilon=0.1^2$	$\varepsilon=1^2$	$\varepsilon=0.01^2$	$\varepsilon=0.1^2$	$\varepsilon=1^2$	$\varepsilon=0.01^2$	$\varepsilon=0.1^2$	$\varepsilon=1^2$	$\varepsilon=0.01^2$	$\varepsilon=0.1^2$	$\varepsilon=1^2$	$\varepsilon=0.01^2$	$\varepsilon=0.1^2$	$\varepsilon=1^2$
ITS	[49]	0.2019	0.1941	0.1832	5.19	4.07	3.29	0.06	0.07	0.08	0.5632	0.5514	0.5405	1.13	1.76	1.91	27.39	25.46	23.44	0.7433	0.7315	0.7268	16.19	17.49	18.34	0.7729	0.7533	0.7417	0.8356	0.8543	0.8739
	[50]	0.2145	0.2011	0.1928	6.57	4.35	3.79	0.06	0.07	0.08	0.6148	0.6064	0.5931	1.01	1.34	1.73	29.11	27.61	25.33	0.7582	0.7439	0.7319	14.42	15.63	16.19	0.7815	0.7769	0.7691	0.8195	0.8308	0.8655
	[61]	0.2218	0.2078	0.1986	6.85	4.73	3.88	0.04	0.06	0.08	0.6508	0.6315	0.6125	0.09	1.11	1.42	30.52	28.73	27.52	0.7835	0.7628	0.7505	13.62	14.85	15.76	0.8041	0.7938	0.8018	0.7959	0.8173	0.8347
	[51]	0.2563	0.2292	0.2058	6.97	5.58	4.24	0.04	0.06	0.07	0.6929	0.6861	0.6786	0.09	1.03	1.17	30.75	29.45	29.21	0.7946	0.7735	0.7661	10.52	11.47	13.49	0.8153	0.8054	0.7961	0.7325	0.7673	0.8034
	[52]	0.5092	0.4814	0.4469	7.08	5.61	4.89	0.03	0.04	0.06	0.8153	0.8026	0.7997	0.53	0.98	1.08	32.94	32.05	31.67	0.8042	0.8002	0.7952	9.17	10.38	12.08	0.8572	0.8447	0.8365	0.6853	0.7153	0.7549
	[37]	0.2961	-	-	4.99	-	-	0.04	-	-	0.6935	-	-	0.94	-	-	29.81	-	-	0.7928	-	-	10.92	-	-	0.8264	-	-	0.5334	-	-
	[39]	0.5093	-	-	5.89	-	-	0.03	-	-	0.8286	-	-	0.71	-	-	32.44	-	-	0.8124	-	-	10.12	-	-	0.8376	-	-	0.5064	-	-
	[41]	0.5468	-	-	6.34	-	-	0.04	-	-	0.8549	-	-	0.43	-	-	32.8	-	-	0.8305	-	-	9.84	-	-	0.8546	-	-	0.4759	-	-
	[40]	0.6115	-	-	6.55	-	-	0.03	-	-	0.9007	-	-	0.4	-	-	34.05	-	-	0.8365	-	-	9.15	-	-	0.8813	-	-	0.4522	-	-
	RMWEF	0.7282	0.6855	0.6226	9.85	8.73	7.52	0.01	0.03	0.04	0.9682	0.9451	0.9305	0.21	0.56	0.87	38.49	36.16	33.71	0.8767	0.8698	0.8505	6.72	8.59	10.27	0.9438	0.8991	0.9168	0.4392	0.6108	0.6846
OTS	[49]	0.1739	0.1522	0.1484	4.91	3.11	2.88	0.1	0.12	0.15	0.7762	0.7529	0.7411	1.63	1.81	1.97	29.26	28.69	27.85	0.7818	0.7746	0.7628	13.85	15.76	17.61	0.7685	0.7492	0.7374	0.8164	0.8493	0.8662
	[50]	0.1955	0.1831	0.1768	5.34	4.53	3.68	0.09	0.11	0.13	0.8032	0.7922	0.7893	1.38	1.51	1.83	30.79	29.85	28.93	0.7909	0.7811	0.7749	12.14	13.64	15.28	0.7893	0.7654	0.7544	0.7829	0.8056	0.8403
	[61]	0.2305	0.2143	0.1975	5.82	4.96	3.75	0.07	0.09	0.13	0.8258	0.8176	0.7934	1.04	1.34	1.75	30.97	29.98	29.41	0.8015	0.7952	0.7831	10.46	11.72	14.73	0.8034	0.7819	0.7731	0.6861	0.7382	0.7649
	[51]	0.2719	0.2673	0.2582	6.01	5.23	4.85	0.07	0.09	0.11	0.8415	0.8399	0.8167	0.62	0.98	1.42	31.58	30.62	29.83	0.8235	0.8164	0.8053	9.67	10.95	12.21	0.8173	0.8068	0.7963	0.6309	0.6845	0.7281
	[52]	0.3914	0.3851	0.3701	6.76	6.05	5.53	0.04	0.07	0.08	0.8809	0.8752	0.8625	0.36	0.85	1.11	33.75	32.44	31.76	0.8364	0.8198	0.8075	8.56	9.83	11.48	0.8358	0.8251	0.8045	0.5615	0.6692	0.7565
	[37]	0.3371	-	-	4.44	-	-	0.07	-	-	0.8794	-	-	0.76	-	-	30.51	-	-	0.8014	-	-	13.73	-	-	0.7908	-	-	0.5128	-	-
	[39]	0.4973	-	-	5.18	-	-	0.06	-	-	0.8907	-	-	0.54	-	-	32.75	-	-	0.8237	-	-	11.02	-	-	0.8005	-	-	0.4759	-	-
	[41]	0.5367	-	-	4.79	-	-	0.05	-	-	0.9148	-	-	0.32	-	-	33.99	-	-	0.8344	-	-	10.69	-	-	0.8347	-	-	0.4305	-	-
	[40]	0.6108	-	-	5.94	-	-	0.04	-	-	0.9438	-	-	0.29	-	-	34.18	-	-	0.8406	-	-	10.34	-	-	0.8514	-	-	0.4008	-	-
	RMWEF	0.7446	0.7096	0.6918	9.09	8.52	7.49	0.01	0.04	0.06	0.9856	0.9708	0.9652	0.14	0.52	0.83	38.52	37.11	35.02	0.8876	0.8753	0.8662	7.49	8.97	10.35	0.9361	0.9056	0.8875	0.3726	0.5803	0.6338
SOTS	[49]	0.2217	0.2029	0.1937	5.54	4.49	3.52	0.09	0.12	0.13	0.8544	0.8476	0.8349	1.44	2.05	2.21	29.18	28.98	27.81	0.8052	0.7845	0.7712	13.81	14.29	16.32	0.7929	0.7851	0.7749	0.8039	0.8392	0.8576
	[50]	0.2482	0.2258	0.2199	6.28	5.04	4.69	0.08	0.1	0.11	0.8675	0.8561	0.8498	1.12	1.94	2.08	29.73	29.35	28.15	0.7937	0.7883	0.7802	12.35	13.72	14.68	0.8176	0.8072	0.7985	0.7845	0.8015	0.8311
	[61]	0.2973	0.2297	0.2215	7.12	5.84	5.11	0.08	0.09	0.11	0.8893	0.8752	0.8609	1.04	1.73	1.99	29.91	29.49	28.01	0.8225	0.8021	0.7928	11.02	12.57	13.46	0.8322	0.8214	0.8112	0.7269	0.7628	0.8067
	[51]	0.3734	0.3406	0.3241	7.62	6.38	5.94	0.06	0.08	0.1	0.9162	0.9013	0.8997	0.95	1.21	1.78	31.57	30.62	29.89	0.8385	0.8157	0.8088	10.58	11.89	12.51	0.8549	0.8376	0.8238	0.6775	0.7156	0.7553
	[52]	0.4418	0.4151	0.3968	7.95	6.69	6.03	0.05	0.07	0.09	0.9348	0.9305	0.9286	0.58	1.09	1.65	32.09	31.48	30.95	0.8469	0.8253	0.8168	9.49	10.92	11.27	0.8597	0.8466	0.8369	0.6204	0.6917	0.7341
	[37]	0.386	-	-	4.83	-	-	0.08	-	-	0.8934	-	-	1.11	-	-	30.86	-	-	0.8164	-	-	13.42	-	-	0.8347	-	-	0.5873	-	-
	[39]	0.4618	-	-	5.78	-	-	0.06	-	-	0.9474	-	-	0.65	-	-	33.47	-	-	0.8256	-	-	10.92	-	-	0.8567	-	-	0.4758	-	-
	[41]	0.5973	-	-	6.65	-	-	0.05	-	-	0.9448	-	-	0.6	-	-	33.82	-	-	0.8418	-	-	10.07	-	-	0.8664	-	-	0.4285	-	-
	[40]	0.6386	-	-	7.34	-	-	0.05	-	-	0.9665	-	-	0.34	-	-	34.24	-	-	0.8638	-	-	10.04	-	-	0.8939	-	-	0.3765	-	-
	RMWEF	0.7863	0.7509	0.7364	9.75	8.45	8.29	0.02	0.03	0.05	0.9992	0.9901	0.9891	0.05	0.38	1.11	36.19	35.62	34.49	0.8745	0.8609	0.8583	5.34	7.15	9.81	0.9547	0.9372	0.9247	0.3595	0.5061	0.5984
RTTS	[49]	0.2775	0.2643	0.2579	4.97	3.22	3.05	0.05	0.08	0.12	0.8348	0.8231	0.8067	1.53	2.42	2.89	30.53	29.79	29.05	0.7918	0.7734	0.7606	12.81	17.38	19.08	0.8138	0.8005	0.7933	0.8369	0.8682	0.8961
	[50]	0.3062	0.2971	0.2839	5.16	4.13	3.94	0.04	0.06	0.11	0.8575	0.8439	0.8383	1.21	2.14	2.47	31.81	30.89	29.47	0.8005	0.7946	0.7759	13.41	15.72	18.35	0.8199	0.8049	0.8021	0.7853	0.8253	0.8482
	[61]	0.3528	0.3384	0.3173	6.72	4.87	4.21	0.04	0.06	0.09	0.9164	0.8855	0.8619	1.01	1.86	2.31	32.94	31.41	29.76	0.8152	0.8019	0.7943	12.92	14.58	16.41	0.8352	0.8258	0.8142	0.7334	0.7921	0.8154
	[51]	0.4064	0.3968	0.3897	7.45	5.94	4.76	0.04	0.05	0.08	0.9593	0.9445	0.9288	0.83	1.43	1.97	34.27	33.04	32.17	0.8265	0.8143	0.8059	12.05	12.64	14.99	0.8529	0.8373	0.8208	0.6951	0.7534	0.7863
	[52]	0.4251	0.4132	0.4054	7.81	6.35	5.51	0.03	0.04	0.08	0.9746	0.9678	0.9501	0.71	1.05	1.42	35.81	34.57	34.15	0.8491	0.8358	0.8275	11.11	11.95	16.27	0.8762	0.8688	0.8435	0.6148	0.6809	0.6611
	[37]	0.4005	-	-	4.73	-	-	0.05	-	-	0.9905	-	-	1.34	-	-	32.22	-	-	0.8127	-	-	11.45	-	-	0.8637	-	-	0.6192	-	-
	[39]	0.5681	-	-	5.29	-	-	0.04	-	-	0.9628	-	-	0.73	-	-	35.04	-	-	0.8349	-	-	10.97	-	-	0.8833	-	-	0.5347	-	-
	[41]	0.6539	-	-	5.94	-	-	0.04	-	-	0.9863	-	-	0.64	-	-	35.69	-	-	0.8371	-	-	10.25	-	-	0.8914	-	-	0.4531	-	-
	[40]	0.7083	-	-	6.84	-	-	0.03	-	-	0.9844	-	-	0.48	-	-	36.19	-	-	0.8409	-	-	9.64	-	-	0.9025	-	-	0.4115	-	-
	RMWEF	0.8072	0.7649	0.7502	9.91	8.18	6.31	0.01	0.02	0.03	0.9981	0.9905	0.9876	0.18	0.44	0.73	38.45	36.79	36.07	0.8752	0.8619	0.8564	7.83	10.43	11.95	0.9772	0.9443	0.9202	0.3502	0.4949	0.6157
HSTS	[49]	0.3492	0.3249	0.3197	5.38	4.64	3.82	0.07	0.1	0.12	0.7738	0.7622	0.7563	1.43	1.97	2.23	30.71	28.65	27.83	0.8115	0.7946	0.7867	11.41	12.38	15.65	0.8278	0.8064	0.7967	0.7859	0.8035	0.8291
	[50]	0.3717	0.3581	0.3367	4.82	4.01	3.67	0.05	0.09	0.11	0.8015	0.7964	0.7805	1.11	1.51	1.95	31.59	29.78	29.13	0.8292	0.8134	0.8009	10.82	11.69	13.78	0.8301	0.8235	0.8152	0.7404	0.7841	0.8017
	[61]	0.4961	0.4427	0.4061	5.75	4.58	4.33	0.05	0.09	0.11	0.8238	0.8194	0.7892	0.95	1.19	1.87	32.45	30.18	29.79	0.8357	0.8253	0.8124	9.59	10.45	11.57	0.8525	0.8438	0.8276	0.7169	0.7526	0.7753
	[51]	0.5953	0.5718	0.5429	5.98	5.23	4.81	0.03	0.07	0.09	0.8519	0.8492	0.8379	0.44	1.01	1.21	33.83	32.53	31.48	0.8438	0.8346	0.8262	8.71	9.78	11.62	0.8662	0.8549	0.8395	0.6792	0.7205	0.7438
	[52]	0.7145	0.7005	0.6673	6.64	5.91	5.29	0.03	0.06	0.08	0.9246	0.9141	0.9073	0.21	0.98	1.08	34.08	33.91	32.85	0.8609	0.8527	0.8497	8.01	8.97	10.31	0.8845	0.8786	0.8559	0.5693	0.6548	0.7025
	[37]	0.6559	-	-	4.95	-	-	0.07	-	-	0.8559	-	-	0.52	-	-	33.48	-	-	0.8249	-	-	10.38	-	-	0.8569	-	-	0.5548	-	-
	[39]	0.7264	-	-	5.68	-	-	0.05	-	-	0.9342	-	-	0.31	-	-	34.04	-	-	0.8465	-	-	9.91	-	-	0.876	-	-	0.4625	-	-
	[41]	0.7005	-	-	6.66	-	-	0.05	-	-	0.9581	-	-	0.24	-	-	34.56	-	-	0.8509	-	-	9.54	-	-	0.8973	-	-	0.4625	-	-
	[40]	0.7387	-	-	6.9	-	-	0.05	-	-	0.9733	-	-	0.16	-	-	35.64	-	-	0.8544	-	-	8.64	-	-	0.899	-	-	0.3517	-	-
	RMWEF	0.8592	0.8097	0.7735	9.92	8.68	8.05	0.01	0.03	0.05	0.9957	0.9811	0.9712	0.07	0.19	0.23	38.85	37.11	36.67	0.8891	0.8749	0.8685	5.75	9.52	8.49	0.9527	0.9331	0.9173	0.3346	0.4396	0.5115

∗ GIF [49]; WGIF [50]; EPDSID [61]; GGIF [51]; EGIF [52]; DN [37]; RYF-Net [39]; PMHLD [41]; IDNPAB [40].

∗ Image dehazing methods which are independent of the regularization parameter (ε) are marked with a dash ($-$) in this Table.

∗ ITS : Indoor Training Set (1200 Images), OTS : Outdoor Training Set (1500 Images), SOTS : Synthetic Objective Testing Set (1000 Images), RTTS : Real-world Task-driven Testing Set (600 Images), HSTS : Hybrid Subjective Testing Set (20 Images).

TABLE 5.2: Comparison of the average performance metrics and execution time using different dehazing methods for three different ε values $(0.01^2, 0.1^2, 1^2)$ and fixed $\zeta_1 = 60$ for Fattal, D-HAZY, Middlebury, NYU and FRIDA Dataset.

Non-Reference Metrics

Datasets	Methods	e ($\varepsilon = 0.01^2$)	e ($\varepsilon = 0.1^2$)	e ($\varepsilon = 1^2$)	$\overline{r}$ ($\varepsilon = 0.01^2$)	$\overline{r}$ ($\varepsilon = 0.1^2$)	$\overline{r}$ ($\varepsilon = 1^2$)	$\overline{\alpha}$ ($\varepsilon = 0.01^2$)	$\overline{\alpha}$ ($\varepsilon = 0.1^2$)	$\overline{\alpha}$ ($\varepsilon = 1^2$)	CNI ($\varepsilon = 0.01^2$)	CNI ($\varepsilon = 0.1^2$)	CNI ($\varepsilon = 1^2$)	FADE ($\varepsilon = 0.01^2$)	FADE ($\varepsilon = 0.1^2$)	FADE ($\varepsilon = 1^2$)
Fattal	[49]	0.2327	0.2008	0.1821	3.67	2.82	1.04	0.07	0.09	0.11	0.8429	0.8169	0.7951	1.21	1.59	2.38
	[50]	0.2608	0.2361	0.2235	4.82	3.35	2.52	0.06	0.08	0.11	0.8618	0.8352	0.8168	1.05	1.16	2.07
	[61]	0.3511	0.2746	0.2482	4.95	3.76	2.84	0.06	0.08	0.09	0.8739	0.8466	0.8247	0.98	1.09	1.86
	[51]	0.3928	0.4137	0.3753	6.14	4.68	3.02	0.05	0.07	0.09	0.8942	0.8508	0.8325	0.91	1.01	1.32
	[52]	0.5001	0.4375	0.4084	6.75	5.42	3.97	0.04	0.07	0.08	0.9068	0.8793	0.8518	0.63	0.99	1.11
	[37]	0.4917	-	-	2.19	-	-	0.06	-	-	0.8592	-	-	1.01	-	-
	[39]	0.5625	-	-	2.78	-	-	0.05	-	-	0.8793	-	-	0.97	-	-
	[41]	0.5096	-	-	2.99	-	-	0.04	-	-	0.8904	-	-	0.64	-	-
	[40]	0.6179	-	-	3.08	-	-	0.03	-	-	0.8965	-	-	0.41	-	-
	RMWEF	0.7063	0.6527	0.6095	8.68	6.37	5.76	0.01	0.04	0.06	0.9658	0.9449	0.9157	0.13	0.52	0.69
D-HAZY	[49]	0.2339	0.2028	0.1715	4.25	2.78	2.85	0.08	0.11	0.13	0.8655	0.8362	0.8035	1.21	1.85	1.79
	[50]	0.2486	0.2362	0.2099	5.18	3.02	2.56	0.08	0.09	0.11	0.8814	0.8625	0.8357	1.09	1.26	1.55
	[61]	0.2641	0.2573	0.2264	5.73	3.85	2.99	0.06	0.09	0.11	0.9005	0.8811	0.8558	1.02	1.11	1.34
	[51]	0.3682	0.3417	0.3083	6.91	4.15	3.11	0.05	0.08	0.1	0.9169	0.9057	0.8769	0.83	0.98	1.15
	[52]	0.5134	0.4904	0.4628	6.96	4.87	4.21	0.04	0.06	0.09	0.9351	0.9099	0.8972	0.58	0.86	1.07
	[37]	0.3681	-	-	3.52	-	-	0.07	-	-	0.8737	-	-	0.72	-	-
	[39]	0.4227	-	-	3.91	-	-	0.04	-	-	0.9005	-	-	0.44	-	-
	[41]	0.5569	-	-	4.14	-	-	0.03	-	-	0.9381	-	-	0.38	-	-
	[40]	0.579	-	-	4.58	-	-	0.04	-	-	0.9577	-	-	0.21	-	-
	RMWEF	0.7315	0.7119	0.6937	8.85	6.91	5.47	0.01	0.02	0.04	0.9855	0.9546	0.9259	0.07	0.38	0.86
Middlebury	[49]	0.2352	0.2141	0.1807	4.76	4.35	3.07	0.06	0.09	0.11	0.8492	0.8346	0.7925	1.61	1.84	2.49
	[50]	0.2508	0.2322	0.2054	5.92	4.83	3.76	0.06	0.09	0.11	0.8681	0.8475	0.8095	1.23	1.67	2.15
	[61]	0.3662	0.2875	0.2368	5.98	4.97	4.12	0.04	0.08	0.09	0.8773	0.8509	0.8167	1.05	1.43	2.05
	[51]	0.3834	0.3609	0.3351	6.55	5.07	4.66	0.04	0.07	0.09	0.9012	0.8764	0.8428	0.91	1.11	1.86
	[52]	0.6149	0.5984	0.5468	7.42	6.65	5.48	0.03	0.05	0.08	0.9383	0.9225	0.8966	0.58	0.97	1.61
	[37]	0.4934	-	-	4.79	-	-	0.07	-	-	0.8889	-	-	1.05	-	-
	[39]	0.5341	-	-	5.07	-	-	0.06	-	-	0.9361	-	-	0.75	-	-
	[41]	0.6507	-	-	5.38	-	-	0.04	-	-	0.9404	-	-	0.44	-	-
	[40]	0.6775	-	-	5.76	-	-	0.05	-	-	0.9655	-	-	0.28	-	-
	RMWEF	0.8215	0.7956	0.7253	9.38	7.35	6.95	0.01	0.04	0.06	0.9965	0.9843	0.9911	0.14	0.53	0.95
NYU	[49]	0.3603	0.3375	0.3104	4.73	3.27	2.56	0.06	0.11	0.11	0.8936	0.8869	0.8444	1.32	1.95	2.37
	[50]	0.3818	0.3584	0.3396	4.59	3.86	3.32	0.06	0.1	0.11	0.9002	0.8914	0.8568	1.14	1.51	2.13
	[61]	0.4841	0.4094	0.3645	5.37	4.02	3.89	0.05	0.09	0.09	0.9252	0.9126	0.8894	1.07	1.35	1.94
	[51]	0.5019	0.4972	0.4624	5.98	4.79	3.45	0.05	0.08	0.08	0.9568	0.9384	0.9168	0.99	1.13	1.51
	[52]	0.5924	0.5635	0.5482	6.62	5.35	4.66	0.04	0.07	0.07	0.9776	0.9508	0.9237	0.63	1.07	1.21
	[37]	0.5144	-	-	4.87	-	-	0.06	-	-	0.9358	-	-	1.03	-	-
	[39]	0.568	-	-	5.61	-	-	0.05	-	-	0.9701	-	-	0.73	-	-
	[41]	0.6819	-	-	5.96	-	-	0.04	-	-	0.9764	-	-	0.51	-	-
	[40]	0.7005	-	-	6.03	-	-	0.04	-	-	0.9886	-	-	0.34	-	-
	RMWEF	0.7792	0.7438	0.7001	9.24	8.75	6.52	0.01	0.03	0.05	0.9969	0.9759	0.9571	0.08	0.72	1.01
FRIDA	[49]	0.3421	0.3219	0.2963	3.63	3.05	2.31	0.07	0.08	0.1	0.8809	0.8535	0.8173	1.31	1.98	3.82
	[50]	0.4137	0.3842	0.3537	3.85	3.52	2.99	0.07	0.08	0.09	0.8975	0.8741	0.8456	1.11	1.76	2.95
	[61]	0.4462	0.4015	0.3823	4.92	3.95	3.15	0.06	0.07	0.09	0.9168	0.8849	0.8578	0.96	1.43	2.51
	[51]	0.4913	0.4627	0.4562	5.25	4.46	3.95	0.06	0.07	0.08	0.9389	0.9173	0.8895	0.75	1.13	2.24
	[52]	0.5602	0.5391	0.5078	6.71	5.35	4.64	0.05	0.06	0.07	0.9573	0.9315	0.9073	0.51	1.02	1.18
	[37]	0.4914	-	-	3.87	-	-	0.06	-	-	0.9148	-	-	0.51	-	-
	[39]	0.5664	-	-	4.25	-	-	0.07	-	-	0.9553	-	-	0.49	-	-
	[41]	0.5938	-	-	4.66	-	-	0.05	-	-	0.9745	-	-	0.36	-	-
	[40]	0.6017	-	-	5.06	-	-	0.04	-	-	0.9884	-	-	0.29	-	-
	RMWEF	0.8195	0.7805	0.7371	9.53	8.08	6.38	0.01	0.04	0.05	0.9987	0.9809	0.9536	0.13	0.79	0.83

Reference Metrics and Execution Time

Datasets	Methods	PSNR ($\varepsilon = 0.01^2$)	PSNR ($\varepsilon = 0.1^2$)	PSNR ($\varepsilon = 1^2$)	SSIM ($\varepsilon = 0.01^2$)	SSIM ($\varepsilon = 0.1^2$)	SSIM ($\varepsilon = 1^2$)	CIEDE2000 ($\varepsilon = 0.01^2$)	CIEDE2000 ($\varepsilon = 0.1^2$)	CIEDE2000 ($\varepsilon = 1^2$)	UIQI ($\varepsilon = 0.01^2$)	UIQI ($\varepsilon = 0.1^2$)	UIQI ($\varepsilon = 1^2$)	Execution Time T/s ($\varepsilon = 0.01^2$)	Execution Time T/s ($\varepsilon = 0.1^2$)	Execution Time T/s ($\varepsilon = 1^2$)
Fattal	[49]	29.48	28.37	26.81	0.7703	0.7591	0.7409	12.39	15.91	16.05	0.8216	0.8006	0.7839	0.7691	0.8262	0.8644
	[50]	30.12	29.45	27.56	0.7769	0.7641	0.7553	11.56	13.85	15.73	0.8349	0.8193	0.8045	0.7245	0.7873	0.8209
	[61]	30.38	29.81	28.92	0.7941	0.7895	0.7738	11.24	13.08	15.56	0.8562	0.8275	0.8091	0.6977	0.7561	0.8042
	[51]	31.17	30.39	29.46	0.7997	0.7903	0.7861	10.63	12.73	14.81	0.8673	0.8511	0.8224	0.6504	0.7359	0.7765
	[52]	33.92	32.55	30.81	0.8305	0.8265	0.8027	9.58	11.45	13.01	0.8955	0.8764	0.8451	0.6053	0.6981	0.7468
	[37]	30.05	-	-	0.8028	-	-	12.76	-	-	0.8539	-	-	0.4509	-	-
	[39]	32.81	-	-	0.8185	-	-	13.22	-	-	0.8581	-	-	0.4009	-	-
	[41]	33.64	-	-	0.8353	-	-	11.94	-	-	0.8694	-	-	0.4055	-	-
	[40]	35.29	-	-	0.8429	-	-	10.73	-	-	0.8857	-	-	0.3841	-	-
	RMWEF	37.44	35.91	32.67	0.8945	0.8657	0.8368	7.84	9.76	11.61	0.9561	0.9246	0.8868	0.3589	0.5507	0.7249
D-HAZY	[49]	31.59	25.69	22.78	0.7652	0.7439	0.7193	11.37	13.64	15.29	0.7953	0.7735	0.7506	0.9106	0.9373	0.9365
	[50]	33.28	27.79	25.93	0.7769	0.7676	0.7468	10.29	11.49	13.75	0.8164	0.8001	0.7887	0.8885	0.9135	0.9025
	[61]	33.64	29.59	27.81	0.8075	0.7843	0.7625	10.01	11.13	13.51	0.8305	0.8157	0.8015	0.8462	0.8843	0.8964
	[51]	34.73	32.71	30.94	0.8115	0.8001	0.7892	9.55	10.84	12.29	0.8518	0.8333	0.8164	0.8115	0.8635	0.8701
	[52]	35.92	33.99	31.58	0.8509	0.8246	0.8067	8.97	10.12	11.97	0.8752	0.8591	0.8319	0.7738	0.8307	0.8539
	[37]	31.82	-	-	0.8194	-	-	11.88	-	-	0.8464	-	-	0.7864	-	-
	[39]	31.19	-	-	0.8125	-	-	10.34	-	-	0.8641	-	-	0.4053	-	-
	[41]	32.28	-	-	0.8209	-	-	10.11	-	-	0.8882	-	-	0.4431	-	-
	[40]	33.05	-	-	0.8379	-	-	10.01	-	-	0.8933	-	-	0.4028	-	-
	RMWEF	37.66	35.19	33.79	0.8753	0.8576	0.8352	6.41	8.95	10.04	0.9485	0.9152	0.8869	0.3971	0.5837	0.6345
Middlebury	[49]	30.73	29.76	26.24	0.7924	0.7758	0.7649	13.38	14.82	16.97	0.8273	0.8135	0.7812	0.9456	1.2505	1.2138
	[50]	31.68	28.52	27.93	0.8015	0.7862	0.7705	11.76	12.05	14.65	0.8439	0.8302	0.8011	0.9231	1.1113	1.0805
	[61]	33.54	30.18	28.46	0.8162	0.7934	0.7756	10.34	11.89	13.71	0.8508	0.8397	0.8075	0.9152	1.0537	0.9989
	[51]	33.69	31.48	29.83	0.8259	0.8067	0.7861	9.87	11.15	12.94	0.8644	0.8459	0.8238	0.8868	0.9519	0.9693
	[52]	34.46	33.81	30.15	0.8344	0.8292	0.8049	9.12	10.28	11.66	0.8829	0.8681	0.8493	0.8449	0.9176	0.9481
	[37]	32.25	-	-	0.8179	-	-	12.58	-	-	0.8547	-	-	0.8429	-	-
	[39]	33.17	-	-	0.8066	-	-	11.05	-	-	0.8708	-	-	0.8016	-	-
	[41]	33.69	-	-	0.8139	-	-	10.88	-	-	0.8937	-	-	0.7405	-	-
	[40]	34.08	-	-	0.8224	-	-	10.16	-	-	0.9246	-	-	0.6924	-	-
	RMWEF	37.82	35.05	33.75	0.8606	0.8478	0.8235	6.05	8.75	9.13	0.9649	0.9424	0.9081	0.6702	0.7554	0.9105
NYU	[49]	29.23	27.42	24.61	0.8268	0.8143	0.8076	11.31	12.92	15.75	0.8352	0.8107	0.8068	0.9943	1.1142	1.2209
	[50]	30.52	29.63	26.76	0.8306	0.8195	0.7973	10.56	12.64	14.34	0.8561	0.8336	0.8219	0.9618	1.0959	1.1715
	[61]	31.73	29.95	27.58	0.8358	0.8211	0.8146	10.03	11.85	13.99	0.8628	0.8415	0.8344	0.9359	0.9978	1.0582
	[51]	32.92	30.16	28.65	0.8471	0.8298	0.8175	9.73	10.36	11.72	0.8902	0.8645	0.8426	0.9135	0.9583	0.9871
	[52]	33.73	31.48	29.92	0.8504	0.8365	0.8242	9.51	9.22	10.04	0.8967	0.8734	0.8505	0.8801	0.9264	0.9804
	[37]	29.79	-	-	0.8148	-	-	11.31	-	-	0.8631	-	-	0.8651	-	-
	[39]	31.11	-	-	0.8054	-	-	12.35	-	-	0.8568	-	-	0.8279	-	-
	[41]	32.58	-	-	0.8136	-	-	11.73	-	-	0.8694	-	-	0.8022	-	-
	[40]	32.65	-	-	0.8191	-	-	10.55	-	-	0.8973	-	-	0.7614	-	-
	RMWEF	34.67	36.64	32.76	0.8873	0.8609	0.8574	5.21	6.46	8.94	0.9462	0.9035	0.8849	0.7466	0.8539	0.9362
FRIDA	[49]	32.19	30.01	29.17	0.8039	0.7918	0.7761	12.18	14.33	16.65	0.8315	0.8162	0.7904	0.9852	1.2062	1.2549
	[50]	33.27	32.46	30.31	0.8121	0.8009	0.7843	11.69	13.59	15.05	0.8576	0.8355	0.8113	0.9349	1.1105	1.1881
	[61]	33.54	32.77	30.98	0.8296	0.8085	0.7921	10.85	12.46	14.81	0.8709	0.8538	0.8394	0.9178	0.9951	1.0162
	[51]	34.98	33.39	31.58	0.8344	0.8213	0.8046	10.07	11.78	12.99	0.8852	0.8761	0.8575	0.8866	0.9325	0.9904
	[52]	35.43	34.16	32.49	0.8531	0.8357	0.8219	9.97	10.25	11.47	0.9011	0.8825	0.8658	0.8351	0.8802	0.9521
	[37]	34.61	-	-	0.8235	-	-	11.94	-	-	0.8558	-	-	0.824	-	-
	[39]	31.57	-	-	0.8209	-	-	11.06	-	-	0.8625	-	-	0.7684	-	-
	[41]	33.68	-	-	0.8255	-	-	10.83	-	-	0.9034	-	-	0.7257	-	-
	[40]	34.45	-	-	0.8347	-	-	10.27	-	-	0.9278	-	-	0.7005	-	-
	RMWEF	39.51	36.05	35.75	0.8762	0.8561	0.8458	5.41	8.62	10.31	0.9771	0.9556	0.9325	0.6937	0.8135	0.8544

∗ GIF [49]; WGIF [50]; EPDSID [61]; GGIF [51]; EGIF [52]; DN [37]; RYF-Net [39]; PMHLD [41]; IDNPAB [40].

∗ Image dehazing methods which are independent of the regularization parameter (ε) are marked with a dash ($-$) in this Table.

∗ Fattal dataset : (12 Synthetic Images), D-HAZY dataset : (350 Hazy Images), Middlebury dataset : (200 Synthetic Images), NYU dataset : (1000 Hazy images), FRIDA dataset : (420 Synthetic Images)

5.4 Limitations

Single image dehazing has been a challenging task due to its ill-posed nature. In this method, a robust multi-scale weighting based edge-smoothing filter (RMWEF) is proposed for single image dehazing. It removes morphological artifacts strongly and preserves fine structures well by choosing a large window radius ζ_1 as 60. However, strong texture and low resolution based hazy images get darkened in the sharp regions.

5.5 Concluding Remarks

Dark channel prior (DCP) is a very standard algorithm to dehaze images. However, it suffers with morphological artifacts. In order to reduce such artifacts a non-local haze line averaging (NL-HLA) algorithm is adopted in this work and a robust multi-scale weighting-based edge-smoothing filter (RMWEF) is proposed for single image dehazing. In RMWEF, a new multi-scale weighting is incorporated in the cost function of GGIF to refine the transmission map more accurately than the existing dehaze methods. It is a local edge-preserving smoothing filter which removes over-smoothing effect strongly in the areas with fine structures and preserves details in such areas very well at large window radius $\zeta_1 = 60$. As expected, we obtain $a_{x',y'} = 1$ for $\gamma_{x',y'} = 1$ to preserve edge information in sharp regions and it is close to 0 for $\gamma_{x',y'} = 0$ to preserve edge information in flat regions. Next, 1-D illustration between pixel intensity and pixel coordinates in the horizontal as well as in the vertical directions prove that the output pixel values of the proposed method are more closer to the input pixel values even with large ε values than the existing methods.

The effectiveness of the proposed method is tested on about 6618 images using different sets of hazy, non-hazy images from RESIDE dataset and Fattal dataset [16], D-HAZY dataset [65], Middlebury dataset [96], NYU dataset, FRIDA dataset and the results are compared with 9 haze removal methods. The qualitative analysis proves that the proposed method is independent of the nature of image and it performs equally well for hazy and non-hazy images as compared to the existing methods. Next, we have tested and reported the performance of the proposed method using various referenced and non-referenced quantitative metrics. Based on these results, it is evident that the proposed RMWEF performs very well and reduces haze more effectively than the existing GIF [49], WGIF [50], EPDSID [61], GGIF [51], EGIF [52], DN [37], RYF-Net [39], PMHLD [41], IDNPAB [40] methods. Additionally, the proposed method is faster than the existing methods for a given resolution of images.